

# Biocatalytic Foams from Microdroplet-Formulated Self-Assembling Enzymes

Julian S. Hertel, Patrick Bitterwolf, Sandra Kröll, Astrid Winterhalter, Annika J. Weber, Maximilian Grösche, Laurenz B. Walkowsky, Stefan Heißler, Matthias Schwotzer, Christof Wöll, Thomas van de Kamp, Marcus Zuber, Tilo Baumbach, Kersten S. Rabe, and Christof M. Niemeyer\*

Industrial biocatalysis plays an important role in the development of a sustainable economy, as enzymes can be used to synthesize an enormous range of complex molecules under environmentally friendly conditions. To further develop the field, intensive research is being conducted on process technologies for continuous flow biocatalysis in order to immobilize large quantities of enzyme biocatalysts in microstructured flow reactors under conditions that are as gentle as possible in order to realize efficient material conversions. Here, monodisperse foams consisting almost entirely of enzymes covalently linked via SpyCatcher/SpyTag conjugation are reported. The biocatalytic foams are readily available from recombinant enzymes via microfluidic air-in-water droplet formation, can be directly integrated into microreactors, and can be used for biocatalytic conversions after drying. Reactors prepared by this method show surprisingly high stability and biocatalytic activity. The physicochemical characterization of the new materials is described and exemplary applications in biocatalysis are shown using two-enzyme cascades for the stereoselective synthesis of chiral alcohols and the rare sugar tagatose.

proven advantages of biocatalytic processes and the enormous range of available enzymes, the field has the potential to enable the sustainable, “green” production of valuable molecules, such as high-priced products (100 to >1000 \$ kg<sup>-1</sup>) like pharmaceutical active ingredients.<sup>[3,5–7]</sup> To address the main challenges for the advancement of the field, namely the development of enzyme cascades, the standardization of production processes and the implementation of continuous process technology,<sup>[7]</sup> the so-called flow biocatalysis is receiving a lot of attention. In this context, basic concepts of established flow chemistry,<sup>[8]</sup> in which machine-assisted modular chemical synthesis is carried out continuously and compartmentalized in miniaturized reactors, are adapted to the special requirements of biocatalysis.<sup>[9–13]</sup> In particular, large quantities of enzyme biocatalysts must be immobilized in microstructured flow reactors under the gentlest

possible conditions. To meet this demand, our group has recently developed so-called “all-enzyme hydrogels” (AEH) formed by self-assembly of SpyCatcher (SC)/SpyTag (ST)-mediated site-specific enzyme conjugation to produce biocatalytic materials composed

## 1. Introduction

Industrial biocatalysis is widely regarded as a “game changer” for the development of a sustainable economy.<sup>[1–4]</sup> Due to the

J. S. Hertel, P. Bitterwolf, S. Kröll, A. Winterhalter, A. J. Weber, M. Grösche, L. B. Walkowsky, K. S. Rabe, C. M. Niemeyer  
Institute for Biological Interfaces (IBGI)  
Karlsruhe Institute of Technology (KIT)  
Hermann-von-Helmholtz-Platz 1, D-76344 Eggenstein-Leopoldshafen,  
Germany  
E-mail: niemeyer@kit.edu

S. Heißler, M. Schwotzer, C. Wöll  
Institute of Functional Interfaces (IFG)  
Karlsruhe Institute of Technology (KIT)  
Hermann-von-Helmholtz-Platz 1, D-76344 Eggenstein-Leopoldshafen,  
Germany

T. van de Kamp, M. Zuber, T. Baumbach  
Institute for Photon Science and Synchrotron Radiation (IPS)  
Karlsruhe Institute of Technology (KIT)  
D-76344 Eggenstein-Leopoldshafen, Germany

T. van de Kamp, M. Zuber, T. Baumbach  
Laboratory for Applications of Synchrotron Radiation (LAS)  
Karlsruhe Institute of Technology (KIT)  
D-76131 Karlsruhe, Germany

The ORCID identification number(s) for the author(s) of this article can be found under <https://doi.org/10.1002/adma.202303952>

© 2023 The Authors. Advanced Materials published by Wiley-VCH GmbH. This is an open access article under the terms of the Creative Commons Attribution-NonCommercial-NoDerivs License, which permits use and distribution in any medium, provided the original work is properly cited, the use is non-commercial and no modifications or adaptations are made.

DOI: 10.1002/adma.202303952

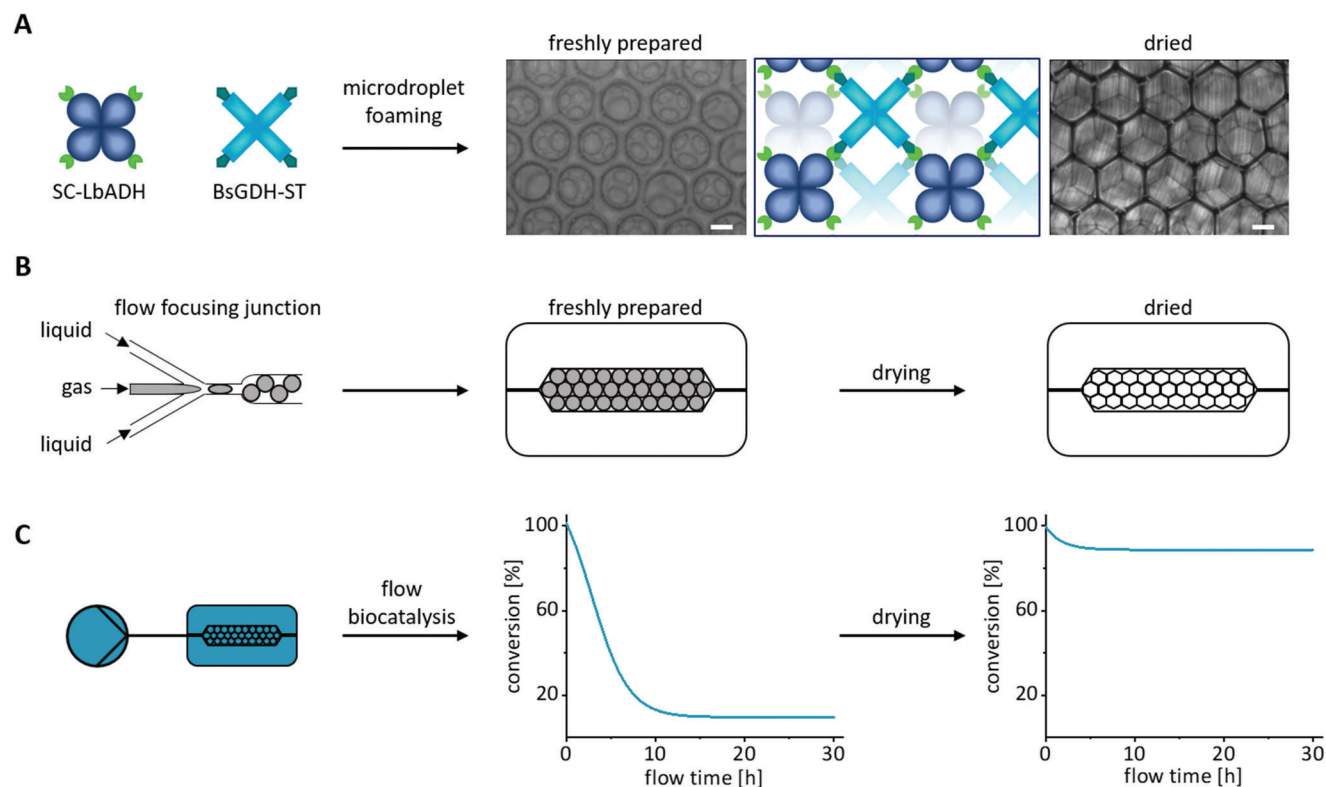


**Figure 1.** Formulation of monodisperse biocatalytic foams. A) Schematic illustration of the formation of a monodisperse protein foam through self-assembly of the two tetrameric enzymes, SC-LbADH (dark blue) and BsGDH-ST (turquoise), in combination with microdroplet foaming. The freshly prepared microbubbles have a spherical shape two minutes after preparation, while after 30 min of drying in air they harden into a porous material with a hexagonal microstructure. Scale bars: 100  $\mu\text{m}$ . B) Schematic illustration of microbubble production by a flow-focusing compound (see Figure S3 (Supporting Information) for details of the setup), which allows the monodisperse foam to be filled directly into microfluidic reactors and dried therein before use in biocatalytic experiments. C) The microfluidic reactors containing the foam were connected to a flow-through system to analyze the biocatalytic conversion of substrates by HPLC. As detailed in section 2.3, comparison of the effect of different drying times showed improved mechanical stability and activity of the foam materials in long-term flow biocatalysis experiments.

almost exclusively of enzymes, thus making optimal use of the available reaction space.<sup>[14]</sup> Later work indicated that AEH can be produced by genetically programmable self-assembly of arbitrary enzymes,<sup>[15–18]</sup> however, monolithic AEH materials have some limitations in terms of diffusion and mass transport within the materials, calling for improved formulations of these powerful biocatalysts.<sup>[19]</sup>

In order to simultaneously maintain the solid anchorage and high enzyme concentration of AEH while still realizing a high surface-to-volume ratio for efficient perfusion and mass transport, we reasoned that these two aspects could be reconciled by foam formulations of AEH. Liquid foams consist of gas bubbles densely packed in a liquid carrier matrix to form a network of gas/liquid interfaces in which merging of the bubbles is prevented by the addition of stabilizing agents such as low molecular weight surfactants, polymers, nanoparticles or mixtures thereof.<sup>[20,21]</sup> Monodisperse foams consisting of bubbles of uniform size can be easily generated via established microfluidic techniques using a T-crossing or a flow-focusing junction,<sup>[22]</sup> and have been used, for instance, to produce biobased liquid foams from alginate or chitosan that can be used as scaffolds for cell culture.<sup>[23,24]</sup> Protein foams are also well known and widely used in the food industry for the uniform introduction of air bubbles

for food texturization. Typically, mixtures of structural proteins such as egg white, gelatin, soy or whey proteins are used for foam production.<sup>[25,26]</sup> During the foaming process, the proteins are concentrated by diffusion to the air/water interface, denature and agglomerate to form a foam-stabilizing film.<sup>[27,28]</sup> Recently, Krause et al. reported that surface-active proteins could be used as a reversible fusion marker for targeted foam enrichment of  $\beta$ -lactamase and thus contribute to the establishment of foam fractionation as a general method for downstream processing of enzymes.<sup>[29]</sup> However, since foaming of catalytically active proteins usually leads to destabilization and inactivation due to protein denaturation at the interfaces,<sup>[30]</sup> biocatalytic applications have been realized only with hybrid foam materials, for instance, by modifying a hybrid silicone foam material with lipases.<sup>[31]</sup>

We here report monodisperse foams composed almost entirely of enzymes covalently linked via SC/ST conjugation (Figure 1). The biocatalytic foams are readily available from recombinant enzymes by microfluidic air-in-water droplet formation and can be directly integrated into microreactors and subsequently dried. The reactors obtained by this method show surprisingly high physical and mechanical stability as well as biocatalytic activity. We describe the physicochemical characterization of the new materials and show exemplary applications in

stereoselective synthesis of chiral alcohols and the rare sugar tagatose.

## 2. Results and Discussion

### 2.1. Microdroplet Formation of Protein Foams

To investigate the possible formation of covalently cross-linked foams by self-assembling enzymes, we used an enzyme system, consisting of a highly (*R*)-selective alcohol dehydrogenase from *Lactobacillus brevis* (LbADH) and nicotinamide adenine dinucleotide phosphate (NADPH)-regenerating glucose-1-dehydrogenase (BsGDH) from *Bacillus subtilis*, which had been extensively characterized from a previous study on the preparation of AEH.<sup>[14]</sup> The two homotetrameric enzymes (Figure 1A) were genetically fused using SC or ST, respectively, as a coupling system, heterologously expressed in *E. coli* cells, purified by Ni-NTA affinity chromatography (Figure S1, Supporting Information), and their kinetic parameters determined (Figure S2, Supporting Information). Equimolar mixing of these proteins leads to the rapid formation of covalent bonds via their SC/ST functionalization<sup>[32]</sup> so that a highly cross-linked system is formed (Figure 1A). As we had shown in a previous work using dynamic light scattering, nanoparticulate aggregates with a diameter of  $\approx 50$  nm initially form in the early phase after mixing (<2 h), which then polymerize into an elastomeric network upon drying in air.<sup>[14]</sup> It should be noted that this network is not a crystal-like structure, but rather an ordered but flexible scaffold due to the conformational flexibility of the protein molecules and the high water content.

To test whether the self-assembling enzyme system is suitable for the production of monodisperse foams, we chose from the multitude of methods known in the literature for microfluidic bubble formation<sup>[20,23,33]</sup> the use of a flow-focusing junction,<sup>[34]</sup> in which two liquid streams and one gas stream meet at the junction, resulting in the formation of monodisperse gas bubbles (Figure 1B). Foaming of an aqueous solution containing equimolar amounts of the two enzymes (1 mM in KMB buffer (100 mM potassium phosphate, pH 7.5, containing 1 mM MgCl<sub>2</sub>)) was performed using a homemade fluidic system fabricated by micromilling and soft-lithography.<sup>[35]</sup> Empirically determined pressures of 450 mbar (liquid) and 400 mbar (gas) were used to ensure the generation of uniform monodisperse bubbles (Figure S3 and Movie S1, Supporting Information). The freshly prepared foam was filled directly into polydimethylsiloxane (PDMS) reactors with a straight reaction channel (27 × 3 × 1 mm) and dried for various defined time intervals to allow formation of the polymeric network. Light microscopic examination of the freshly prepared gas bubbles revealed the structural morphology of densely packed spherical bubbles, which are transformed into a rigid hexagonal lattice by drying (Figure 1A). Reactors containing the foams produced in this way were used directly for flow biocatalysis, showing increased mechanical stability and biocatalytic activity as a result of drying (Figure 1C).

### 2.2. Characterization of Enzyme Foams

An initial more detailed characterization of the foam material was performed using fluorescence microscopy. For this purpose, pro-

tein solutions containing 500  $\mu$ M of each enzyme were mixed with 100  $\mu$ M fluorescein isothiocyanate (FITC) to stain the proteins, then foamed and the freshly prepared material was dried for various times up to 28 days. The freshly foamed materials showed spherical gas-filled bubbles dispersed in a protein solution (Figure 2A, fresh). Already after a drying time of only 30 min (Figure S4, Supporting Information), a change in morphology towards a regular hexagonal network was observed, which remained stable even after a long drying time of 28 days (Figure 2A, 28 d drying). The diameters of the voids formed from the spherical bubbles in the hexagonal honeycomb structure were determined automatically using a Python-based script for  $n \geq 100$  individual bubbles (Figure S5, Supporting Information). The analysis showed that the pore size remained almost stable at  $\approx 180$   $\mu$ m during drying (Figure 2B). However, drying resulted in a notable decrease in the thickness of lamellae between the voids to a value of  $\approx 10$   $\mu$ m, suggesting a densifying packing of the enzymes within the foamed AEH material (Figure S5, Supporting Information). For a first assessment of the mechanical stability of the foam materials, microfluidic reactors containing foams after different drying times were treated under flow conditions with KMB buffer at a flow rate of 1  $\mu$ L min<sup>-1</sup> for 30 h and then reexamined microscopically. Foams that had been dried for only a short time (30 min) collapsed under these conditions, leaving only a thin protein layer at the bottom of the reactor after treatment (Figure 2C, 30 min drying). In contrast, the hexagonal protein structure of the foam dried for 28 days remained largely intact (Figure 2C, 28 d drying), indicating a significantly increased mechanical stability of the material.

Since the fluorescence microscope method described above only allows 2D slice images, we also used laser scanning microscopy (LSM) (Figure 2D) and X-ray tomography (Figure 2E–G) to obtain insights into the 3D structure. Due to the higher time resolution, LSM analyses revealed that some spherical bubbles are still present after only 5 min of drying time, but the hexagonal protein scaffold is already almost fully formed (Figure 2D). In addition to the lamellae, these images also showed the surfaces of the bubbles being under tension and rupturing during drying (Figure 2D, red arrows).

To investigate the deeper 3D structure, which is likely to be responsible for the stability of the material, X-ray tomographic studies were performed on a foam dried for 7 days and taken from a PDMS reactor (Figure 2E). In the volume rendering resulting from the measured data (Figure 2F), uniform cells with dimensions of 500 × 500 × 500  $\mu$ m were defined (Figure 2G) and the average pore size and surface-to-volume were determined based on these cubes (Figure S6, Supporting Information). The resulting size distribution of pore diameters and lamella thicknesses showed an average of 160 and 8  $\mu$ m, respectively, which agrees well with the fluorescence microscopy data (Figures S5 and S6, Supporting Information). The surface-to-volume ratio was found to be  $\approx 45$  m<sup>2</sup> m<sup>-3</sup>. Overall, these studies suggested that the enzyme foams had better diffusion and mass transfer properties within the materials than monolithic AEH materials, which were found to have an average pore size of 200 nm.<sup>[14]</sup>

Since a prolonged drying time does not lead to a change in morphology but still seems to increase mechanical stability (Figure 2C), we determined the amount of water remaining in the protein scaffold after each drying time. To this end, the

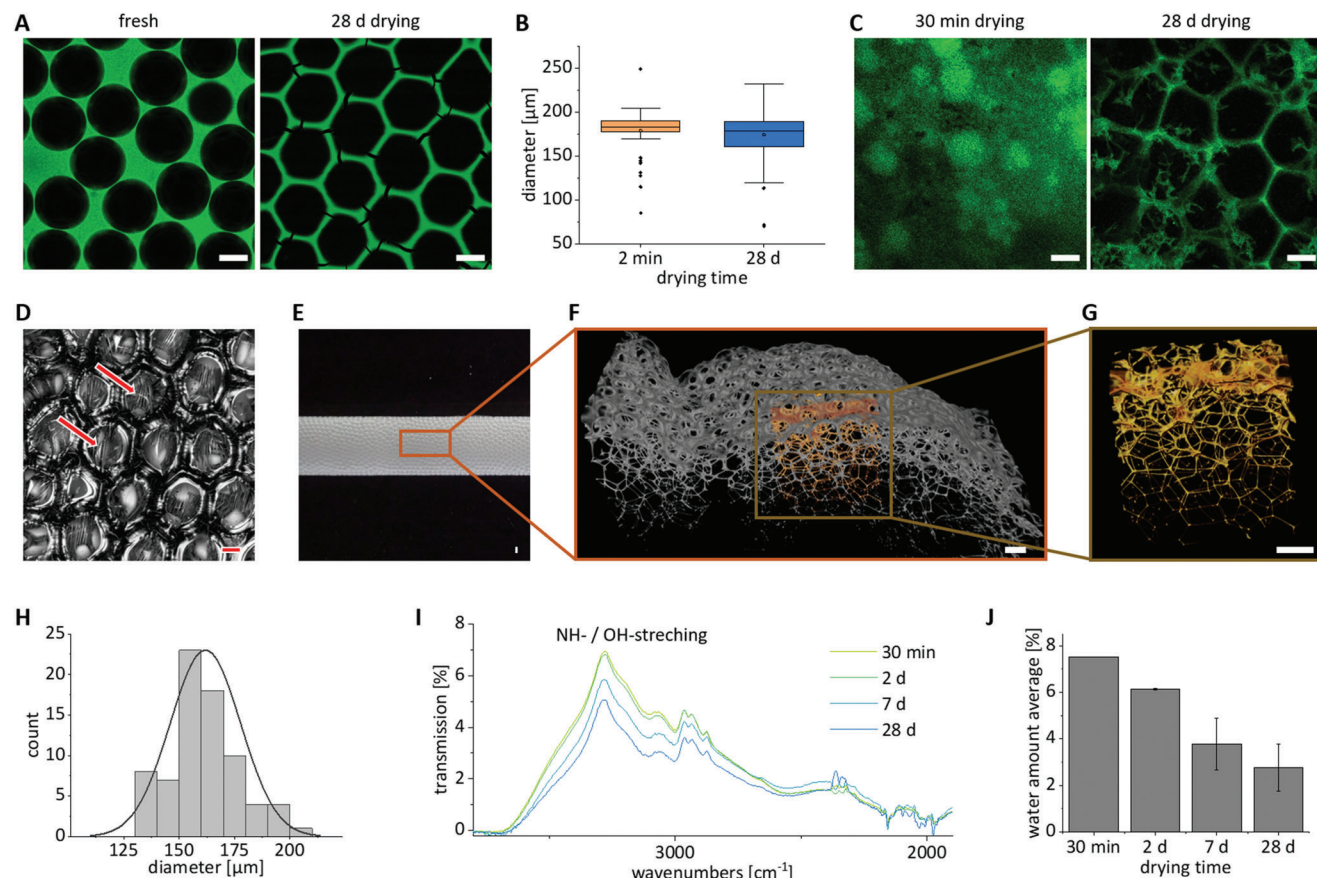


**Figure 2.** Characterization of enzyme foams. A) Fluorescence microscopy of FITC-labeled foam material freshly prepared and dried for 28 d and corresponding pore diameters (B; for details, see Figure S5, Supporting Information). C) Fluorescence micrographs of FITC-labeled foam materials dried for 30 min (left) or 28 d (right) and then perfused with buffer for 30 h. D) Laser scanning micrograph of a top view of a foam dried for 5 min. The arrows indicate places of tension and tearing of the lamellae during drying. E–G) X-ray tomography analysis of 7 d dried foam. Volume rendering of the X-ray tomography of the dried foam (gray) and selection of a unit cell with the edge length of 500  $\mu\text{m}$  (yellow) for the pore diameter analysis. The zoom-in of the unit cell shows the hexagonal shape of the pores within the 3D matrix. All scale bars are 100  $\mu\text{m}$ . H) Pore diameter distribution determined from X-ray tomography data using the Avizo pore-network-model system. I) IR spectra of the OH and NH stretching region of protein foams after different drying times. For complete spectra, see Figure S7 (Supporting Information). J) Average water content of the foam materials calculated from IR and TGA measurements. Sample size (n): B) n = 100, H) n = 75, J) n = 4. Error bars in (J) represent the standard deviation (SD).

relative water content was determined by IR spectroscopy (Figure 2I; see also Figure S7, Supporting Information) and thermogravimetry (TGA, Figure S8, Supporting Information) of enzyme foams after different drying times. The absolute water content of the dried foams was quantified by TGA and IR was also used to determine the relative water content by normalizing to the NH and OH stretching vibrations characteristic of proteins. Both methods independently showed the same relative water contents and confirmed that the amount of water decreased with increasing drying time (Figure 2J). Even after 28 d of drying, the foams still contained  $\approx 40\%$  of the original water content, indicating tightly bound hydrate water in the protein network. IR spectroscopic studies also revealed that the dried foam could be easily rehydrated and returned to the original dried state after re-drying, with no significant differences in the spectra (Figure S7, Supporting Information). Thus, the data obtained show that hydrate water is lost by drying, yet substantial amounts are still present even after 28 d. A longer drying time should increase the concentration of proteins in the lamellar domains and could lead to a denser

packing and/or stronger crosslinking of previously unconnected SC/ST domains, which could account for the observed increase in stability.

### 2.3. Performance of Enzyme Foams in Flow Biocatalysis

We then investigated the performance of the novel enzyme foam materials under flow biocatalysis conditions. For this purpose, a total volume of 1 mL of a 1 mM protein solution was foamed from equimolar amounts of SC-LbADH and BsGDH-ST, distributed among 16 microreactors, resulting in an average loading of each reactor of 62.5  $\mu\text{L}$ , corresponding to a protein amount of 1.25 mg SC-LbADH and 0.97 mg BsGDH-ST per reactor. These reactors were dried for different time intervals (either 30 min, 2, 7, or 28 days) and their biocatalytic performance was investigated in a flow-through reaction setup at different flow rates (Figure 3A; for the detailed setup, see Figure S9, Supporting Information). To analyze the effect of drying on both mechanic

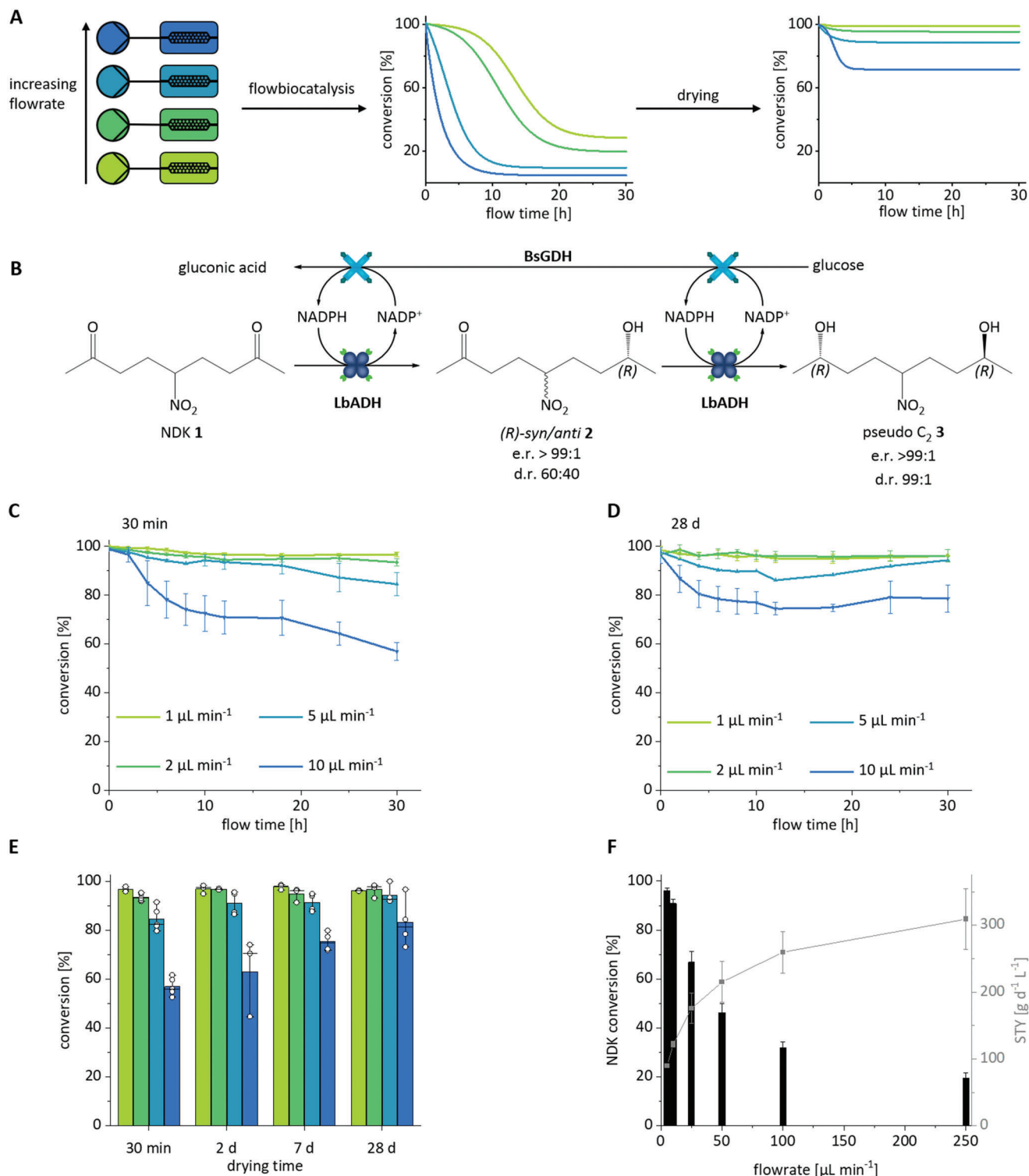


**Figure 3.** Performance of microreactors loaded with dried LbADH/BsGDH protein foams in continuous flow biocatalysis. A) Schematics of experimental study. PDMS-microreactors loaded with enzyme foams were dried for variable times (30 min, 2 d, 7 d, or 28 d) and then analyzed with a model reaction at variable flow rates to the effect of drying on both mechanical stability and enzymatic activity. B) Reaction scheme of the two step (*R*)-selective reduction of the substrate 5-nitrononane-2,8-dione (NDK 1) to the corresponding hydroxyketone 2 and diol 3 products. C,D) NDK conversion over 30 h by enzyme foams dried for 30 min C) and 28 days D) at variable flow rates. For the corresponding analyses of foams dried for 2 d and 7 d, see Figure S11 (Supporting Information). E) Summary of biocatalytic conversion observed after 30 h of continuous catalysis for the different drying times and corresponding flow rates. F) Flowrate dependent productivity of a 7 d dried foam (black) along with the corresponding STY (grey). Sample size (n): C) n = 5, D) n = 4, E) n ≥ 3, F) n = 4. All error bars represent the standard deviation (SD).

stability and enzymatic activity, four reactors of a specific drying time were used for the stereoselective reduction of the substrate 5-nitrononane-2,8-dione (NDK 1) to the corresponding hydroxyketone and diol products by applying four different flow rates (1, 2, 5, and 10  $\mu\text{L min}^{-1}$ ). The model reaction cascade catalyzed by LbADH/BsGDH is shown in Figure 3B.<sup>[36]</sup> All experiments were performed for >30 h in KMB buffer containing 1 mM NADP<sup>+</sup> and 100 mM Glucose, and samples were taken at regular time intervals to quantify products by chiral HPLC analysis (Figure S10, Supporting Information).

The results of the study of the effect of drying on mechanical stability and enzymatic activity are evident from the comparison of the materials dried for 30 min (Figure 3C) and 28 days (Figure 3D). Basically, for all reactors, the nearly complete conversion of the NDK substrate is seen at early time points of the flow biocatalysis, but then drops off at later time points. However, this drop occurs earlier with increasing flow velocity and thus higher mechanical stress on the biomaterial, which favors the flushing of immobilized proteins out of the reactor. For example, in the case of the 30 min material (Figure 3C), 100 % conversion is still observed after 30 h at 1  $\mu\text{L min}^{-1}$  but only  $\approx 60\%$  at 10  $\mu\text{L min}^{-1}$  (Figure 3C). However, a similar comparison only leads to a drop to 80 % at 10  $\mu\text{L min}^{-1}$  for the 28 day material (Figure 3D). This trend, that the enzyme foams have a higher resistance to high flow rates and pressures with increasing drying time, was evident for all materials investigated (Figure 3E, see also Figure S11, Supporting Information). In the case of the 28 day material, this resulted in a highly stable biocatalyst that provided stable, quantitative conversion of the substrate even at high flow rates of 10  $\mu\text{L min}^{-1}$ .

To confirm that this effect was indeed due to SC/ST covalent crosslinking,<sup>[32]</sup> reactors were filled with a foam of SC-LbADH and BsGDH lacking the ST domain and assayed for each drying time at an average flow rate of 5  $\mu\text{L min}^{-1}$  (Figure S12, Supporting Information). As expected, the lack of ST labeling on BsGDH resulted in a strong washout of proteins and thus a rapid decrease in NDK turnover. However, it was also observed that extended drying time resulted in improved performance with still 40% turnover (Figure S12, Supporting Information), as compared to >90% when using the BsGDH-ST enzyme (Figure 3D). These results suggest that the formulation as a foam alone exerts a stabilizing effect on the enzymes, since storage in homogeneous solution leads to no significant residual activity after only 2 days (<4%, see Figure S2C, Supporting Information). To further investigate the mechanical stability, we also performed a characterization of the materials remaining in the reactor after catalysis by staining the remaining protein with fluorescamine (1 mM in KMB buffer) and examining it by fluorescence microscopy (Figure S13, Supporting Information). At shorter drying times (30 min, 2 days), the hexagonal foam structure was completely destroyed during catalysis, leaving only a thin protein layer. In contrast, for longer drying times, intact foam structure was observed even after 30 h of catalysis. In fact, the drying time of 7 days showed the best compromise between stability and time required for drying, so all further experiments were performed with foams dried at 30 °C for 7 days.

Enzyme foams prepared in this way were investigated for their space-time yields (STY) and compared with the previously established monolithic AEH system.<sup>[14]</sup> For this purpose, the re-

actor was operated continuously with gradually increasing flow rates from 5 to 250  $\mu\text{L min}^{-1}$  and the conversion of the NDK (Figure 3F; black bars) and the STYs (Figure 3F; gray curve) were calculated. Compared to the monolithic AEH materials, the larger surface area and pore size of the foams dominate at low flow rates (<20  $\mu\text{L min}^{-1}$ ), leading to an increase in STYs by a factor of 2. However, as the flow rate increases, the higher mechanical stability of the hydrogels plays an increasingly important role, so that at high flow rates of 50  $\mu\text{L min}^{-1}$  the hydrogel and the foam are still almost equal in terms of their space-time yield (hydrogel 250  $\text{g d}^{-1} \text{L}^{-1}$ , foam: 200  $\text{g d}^{-1} \text{L}^{-1}$ ), while at 250  $\mu\text{L min}^{-1}$  the STY of the hydrogel exceeds that of the foam by a factor of 1.5. Due to their improved STY at practical flow rates (e.g., 10  $\mu\text{L min}^{-1}$ ), the foams thus offer significant advantages over monolithic hydrogels, also because the specific activity of the foams (1.38  $\text{mmol}_{\text{product}} \text{mmol}_{\text{enzyme}}^{-1} \text{min}^{-1}$ , 0.0343  $\text{U mg}^{-1}$ ) is  $\approx 2.5$ -fold higher than that of the hydrogels (0.53  $\text{mmol}_{\text{product}} \text{mmol}_{\text{enzyme}}^{-1} \text{min}^{-1}$ , 0.0136  $\text{U mg}^{-1}$ ).

## 2.4. Toward Applications

To investigate the applicability of the enzyme foams for the continuous production of chiral alcohols, we tested whether their use in serial stereoselective biocatalysis was possible. For this purpose, reactors containing SC-LbADH/BsGDH-ST foams were dried for 7 days and perfused successively with three different substrates (5 mM of either NDK 1, acetophenone 4, or chloroacetophenone 6) at a flow rate of 5  $\mu\text{L min}^{-1}$  over several days in iterative cycles. By exchanging the substrate solution every 8 h, a single reactor was able to convert the different substrates into the corresponding (*R*)-alcohols 2, 3, 5, and 7 (Figure 4A). Analysis of the effluents by chiral HPLC clearly showed that the enzyme foams exhibited high degrees of conversion of >95% and stereoselectivity of >99% even after 4 days of continuous conversion, without any decrease in productivity. The result that the enzyme foams exhibited high substrate promiscuity confirmed results obtained with the same enzymes in previous studies.<sup>[14]</sup> Furthermore, their high stability over long periods of time, leading to constant, almost complete conversion even with repeated changes of substrate suggests that the new biocatalytic materials fulfill important practical factors for possible future industrial use. Although substrate concentrations of only 5 mM or less were tested for the LbADH/BsGDH system, substrate concentrations of up to 200 mM were used for tagatose-producing enzyme systems (see below). We have not yet obtained any evidence of practical limitations of the enzyme foams with respect to high substrate concentrations. However, we note that substrate solutions with increased viscosity may lead to more severe mechanical stresses on the foam structures.

To further demonstrate that the novel foam materials can be used for biocatalytic production processes, we chose to produce a challenging product, the rare sugar tagatose.<sup>[37]</sup> Commonly L-arabinose isomerase is being used as either free or immobilized enzyme, or in whole-cell catalysis, to produce D-tagatose by isomerization from D-galactose, leading to productivities for free or immobilized isomerase of 0.3 – 9.6  $\text{g L}^{-1} \text{h}^{-1}$ <sup>[38–42]</sup> and of 0.21 – 1.13  $\text{g L}^{-1} \text{h}^{-1}$  for synthesis by whole-cells.<sup>[37,43,44]</sup>

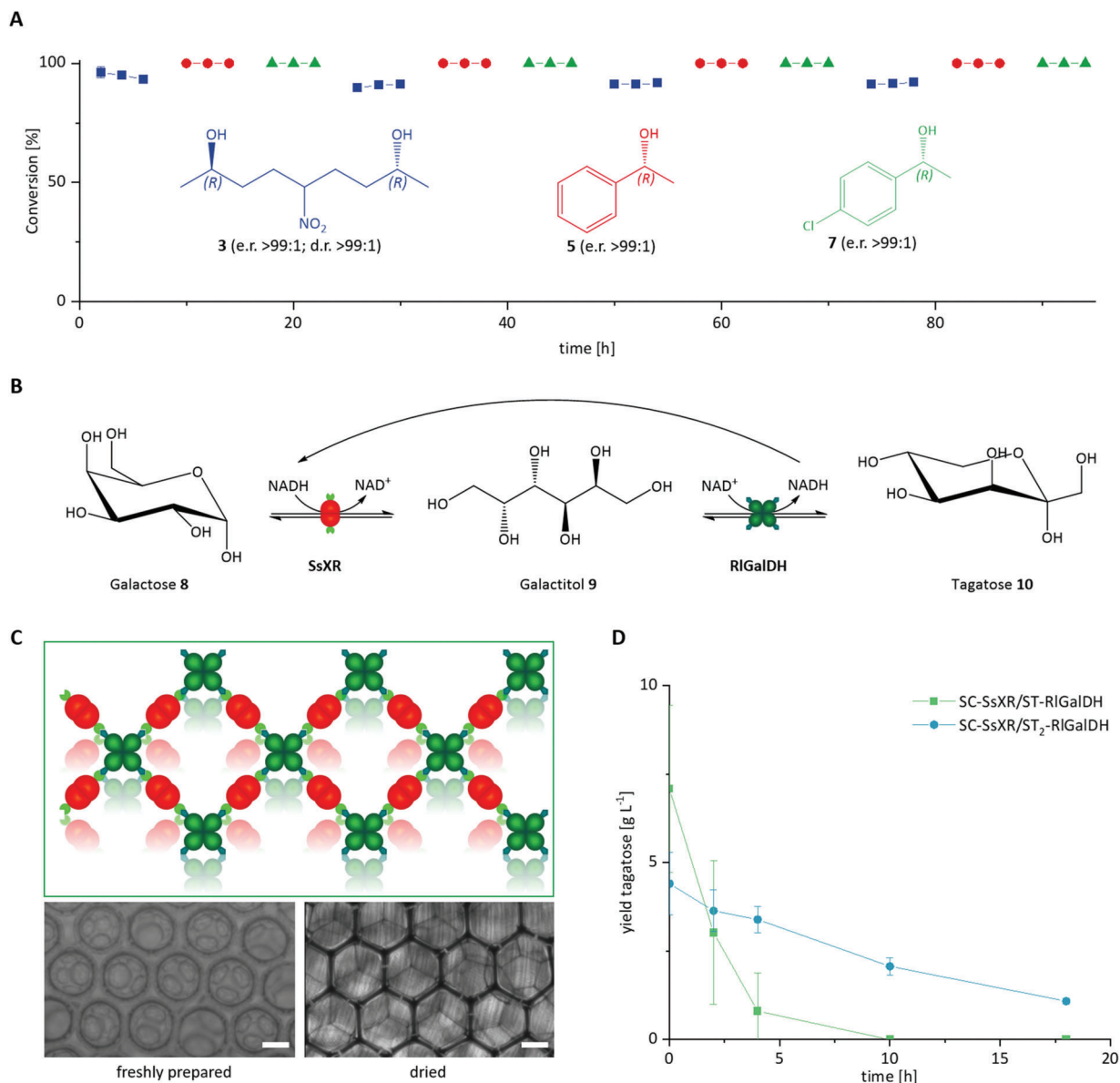


**Figure 4.** Application of enzyme foams for flow biocatalytic synthesis of various products. A) Sequential continuous flow biocatalytic production of the (*R*)-configured hydroxyketone **2** and diol **3** (blue), (*R*)-phenylethanol **5** (red) and (*R*)-4-Chloro- $\alpha$ -methylbenzyl alcohol **7** (green), by use of the LbADH/BsGDH foam. The foam was sequentially perfused with the respective substrate for 8 h each under constant cofactor supply with a flowrate of 5  $\mu\text{L min}^{-1}$ . B) Reaction scheme for the production of the rare sugar tagatose by coupling the conversion of galactose using SsXR (red) under NADH consumption with the conversion of galactitol using RIGalDH (green) under NADH regeneration. C) Schematic structure of the enzyme material (top) and transmitted light microscopy images of a freshly prepared (left) and dried (right) SC-SsXR/ST-RIGalDH foam. Scale bars are 100  $\mu\text{m}$ . D) Production of tagatose using foams consisting of SC-SsXR and ST-RIGalDH or ST<sub>2</sub>-RIGalDH, respectively. Continuous biocatalytic conversion of 7 d dried SsXR/RIGalDH foams in a microfluidic reactor under continuous supply of 200 mM galactose **8** and 3 mM NADH at a flowrate of 1  $\mu\text{L min}^{-1}$ . Note that only the foam using RIGalDH equipped with two sequential N-terminal ST (ST<sub>2</sub>-RIGalDH) led to the production of tagatose for over 18 h. Sample size (n): A) n = 3, D) n  $\geq$  2. All error bars represent the standard deviation (SD).

Recently, oxidoreductive reactions have been used to overcome the thermodynamic equilibrium of the isomerization reaction and to improve the purification of the final product.<sup>[45,46]</sup> Here, we adopted the enzymes of the yeast whole-cell catalytic system consisting of xylose reductase (SsXR) from *Scheffersomyces stipitis* and galactitol dehydrogenase (RIGDH) from *Rhizobium leguminosarum*.<sup>[45]</sup> To produce the foams, the enzymes SsXR and

RIGalDH were fused to SC or ST, respectively, heterologously expressed, purified, the functionality of the SC/ST coupling and the enzymatic activity were verified (Figure S14 and S15 respectively, Supporting Information). Since xylose reductase naturally has a dimeric structure<sup>[47]</sup> and galactitol dehydrogenase forms a tetramer,<sup>[48,49]</sup> cross-linking should result in an alternating structure (Figure 4C).

In an initial flow reaction, a protein foam dried for 7 d consisting of SC-SsXR/ST-RlGalDH was perfused with a continuous supply of 200 mM galactose and 3 mM NADH in a 50 mM Tris-HCl-buffer (pH 8.0) at a flow rate of 1  $\mu\text{L min}^{-1}$  and the effluent was analyzed by HPLC. After very high initial yields of 7  $\text{g L}^{-1}$ , the productivity of the reactor dropped rapidly after  $\approx 10$  h (Figure 4D, green curve). Since we observed a strong washout of the protein material, a second ST domain was added to the RlGalDH to provide additional connection points for stronger cross-linking and thus stabilize the foam. Indeed, this simple adjustment produced a much more stable foam that provided a significant yield of tagatose over 18 h (Figure 4D, blue curve). The initial productivity of 2.9  $\text{g h}^{-1} \text{L}^{-1}$  of ST<sub>2</sub>-RlGalDH is lower than that of ST-RlGalDH, as the introduction of multiple ST domains often leads to loss of activity.<sup>[15]</sup> A direct comparison with previous studies on tagatose synthesis is not possible because no fluidic experiments using the same purified enzyme system have been described. The above whole-cell approach using SsXR and RlGalDH yielded a STY of 3  $\text{g h}^{-1} \text{L}^{-1}$  tagatose,<sup>[45]</sup> which is only slightly higher than the average productivity of our foam reactors. However, since the system described here has not yet been optimized in any way for tagatose production and only the wild-type enzymes have been used so far, we are confident that protein engineering can achieve both higher individual specific activities and stabilization of the intermolecular interactions between the respective subunits to provide a sustainable and efficient synthetic pathway for rare sugar production. As a general remark, we would like to note that at present it is basically impossible to estimate without experimental tests to what extent protein stability can be changed by immobilization, since both positive (stability-increasing) and negative (stability-decreasing) effects can result from immobilization.<sup>[50]</sup> For example, it is very well known that immobilization of enzymes can result in a loss of activity if it limits their molecular flexibility and/or induces (partial) denaturation at the interface.<sup>[30]</sup> As shown in the present example, the enzymes of tagatose synthesis lose their activity in solution after only 2 days at 30 °C, whereas it is retained in the foams. We therefore assume that in our approach the flexibility of the proteins is preserved, since no rigid abiotic surfaces are used, but only hydrated protein structures, which provide protection against harmful interactions with the substrate liquid and thus stabilize the structure and activity of the individual embedded enzymes.

### 3. Conclusion

In summary, our work shows for the first time that the formulation of enzymes as foams by microdroplet bubble formation leads to biocatalytically active protein materials with high suitability for flow biocatalysis. A physically stable hexagonal honeycomb structure with an average pore diameter of 160  $\mu\text{m}$  and a lamella thickness of 8  $\mu\text{m}$  is formed from the freshly prepared monodisperse spherical bubbles after a few minutes. The biocatalytic foams can be directly integrated into microreactors, ensuring stable immobilization of enzymes in the reactor after drying and allowing them to be used for biocatalytic conversions. The stabilization of the enzymes by drying observed in this work is not only very surprising, since according to the state of research, foaming of proteins leads to their denaturation and inactivation,<sup>[27,28,30]</sup>

but also has high application relevance. Since the foam formulation results in stable, storable reaction systems, the door is open for a wide range of applications in which such systems can be manufactured in large scale and distributed as ready-to-use products. While for small enzymes embedding in water-stable metal-organic-frameworks (MOFs) is an option,<sup>[51]</sup> for larger biocatalysts, such as cascade systems of two or more enzymes, pores with larger dimensions are required to enable efficient and stable process conditions. Since, as shown in the example of tagatose production, the strategy of immobilizing enzymes in the form of biocatalytic foams can be easily transferred to new enzyme systems, we believe that these innovative materials can pave the way to high-performance production systems for industrial biotechnology.

### Supporting Information

Supporting Information is available from the Wiley Online Library or from the author.

### Acknowledgements

This work was supported through the Helmholtz program “Materials Systems Engineering” under the topic “Adaptive and Bioinspired Materials Systems” and the Helmholtz Enterprise project ChemZyme (HE-2020-26). P.B. and A.J.W. were grateful for a Kekulé fellowship by Fonds der Chemischen Industrie. The authors acknowledge the KIT light source for provision of instruments at their beamlines and the Institute for Beam Physics and Technology (IBPT) for operation of Karlsruhe Research Accelerator (KARA) storage ring. The authors thank Elias Hamann for assistance with X-ray measurements and Felix Ott for help with quantitative assessment of enzyme productivity.

Open access funding enabled and organized by Projekt DEAL.

### Conflict of Interest

The authors declare the following competing financial interest(s): The authors declare that a patent application has been filed. P.B., M.G., L.B.W., K.S.R. and C.M.N. declare that they have a competing interest.

### Data Availability Statement

The data that support the findings of this study are available from the corresponding author upon reasonable request.

### Keywords

enzymes, flow biocatalysis, microreactors, monodisperse foams, porous materials

Received: April 27, 2023  
Revised: June 16, 2023  
Published online:

- [1] P. J. Nieuwenhuizen, D. Lyon, *J. Commer. Biotechnol.* **2011**, *17*, 159.  
[2] B. Hauer, *ACS Catal.* **2020**, *10*, 8418.

- [3] S. Wu, R. Snajdrova, J. C. Moore, K. Baldenius, U. T. Bornscheuer, *Angew. Chem. Int. Ed. Engl.* **2021**, *60*, 88.
- [4] E. L. Bell, W. Finnigan, S. P. France, A. P. Green, M. A. Hayes, L. J. Hepworth, S. L. Lovelock, H. Niikura, S. Osuna, E. Romero, K. S. Ryan, N. J. Turner, S. L. Flitsch, *Nat. Rev. Methods Primers* **2021**, *1*, 46.
- [5] R. A. Sheldon, J. M. Woodley, *Chem. Rev.* **2017**, *118*, 801.
- [6] B. Wiltschi, T. Cernava, A. Dennig, M. Galindo Casas, M. Geier, S. Gruber, M. Haberbauer, P. Heidinger, E. Herrero Acero, R. Kratzer, C. Luley-Goedl, C. A. Müller, J. Pitzer, D. Ribitsch, M. Sauer, K. Schmölzer, W. Schnitzhofer, C. W. Sensen, J. Soh, K. Steiner, C. K. Winkler, M. Winkler, T. Wriessnegger, *Biotechnol. Adv.* **2020**, *38*, 107520.
- [7] J. M. Woodley, *Appl. Microbiol. Biotechnol.* **2019**, *103*, 4733.
- [8] S. V. Ley, D. E. Fitzpatrick, R. M. Myers, C. Battilocchio, R. J. Ingham, *Angew. Chem. Int. Ed. Engl.* **2015**, *54*, 10122.
- [9] A. Kchler, M. Yoshimoto, S. Luginbuhl, F. Mavelli, P. Walde, *Nat. Nanotechnol.* **2016**, *11*, 409.
- [10] S. P. France, L. J. Hepworth, N. J. Turner, S. L. Flitsch, *ACS Catal.* **2017**, *7*, 710.
- [11] K. S. Rabe, J. Müller, M. Skoupi, C. M. Niemeyer, *Angew. Chem. Int. Ed. Engl.* **2017**, *56*, 13574.
- [12] J. Britton, S. Majumdar, G. A. Weiss, *Chem. Soc. Rev.* **2018**, *47*, 5891.
- [13] L. Leemans Martin, T. Peschke, F. Venturoni, S. Mostarda, *Curr. Opin. Green Sustain. Chem.* **2020**, *25*, 100350.
- [14] T. Peschke, P. Bitterwolf, S. Gallus, Y. Hu, C. Oelschlaeger, N. Willenbacher, K. S. Rabe, C. M. Niemeyer, *Angew. Chem. Int. Ed. Engl.* **2018**, *57*, 17028.
- [15] P. Bitterwolf, S. Gallus, T. Peschke, E. Mittmann, C. Oelschlaeger, N. Willenbacher, K. S. Rabe, C. M. Niemeyer, *Chem. Sci.* **2019**, *10*, 9752.
- [16] T. Peschke, P. Bitterwolf, S. Hansen, J. Gasmı, K. S. Rabe, C. M. Niemeyer, *Catalysts* **2019**, *9*, 164.
- [17] P. Bitterwolf, F. Ott, K. S. Rabe, C. M. Niemeyer, *Micromachines* **2019**, *10*, 783.
- [18] E. Mittmann, S. Gallus, P. Bitterwolf, C. Oelschlaeger, N. Willenbacher, C. M. Niemeyer, K. S. Rabe, *Micromachines* **2019**, *10*, 795.
- [19] P. Bitterwolf, A. E. Zoheir, J. Hertel, S. Kröll, K. S. Rabe, C. M. Niemeyer, *Chem. Eur. J.* **2022**, *28*, e202202157.
- [20] W. Drenckhan, A. Saint-Jalmes, *Adv. Colloid Interface Sci.* **2015**, *222*, 228.
- [21] W. Drenckhan, S. Hutzler, *Adv. Colloid Interface Sci.* **2015**, *224*, 1.
- [22] P. Garstecki, I. Gitlin, W. DiLuzio, G. M. Whitesides, E. Kumacheva, H. A. Stone, *Appl. Phys. Lett.* **2004**, *85*, 2649.
- [23] S. Andrieux, W. Drenckhan, C. Stubenrauch, *Polymer* **2017**, *126*, 425.
- [24] S. Andrieux, W. Drenckhan, C. Stubenrauch, *Langmuir* **2018**, *34*, 1581.
- [25] P. J. Hailing, P. Walstra, *Crit. Rev. Food Sci. Nutr.* **1981**, *15*, 155.
- [26] P. A. Wierenga, H. Gruppen, *Curr. Opin. Colloid Interface Sci.* **2010**, *15*, 365.
- [27] J. R. Clarkson, Z. F. Cui, R. C. Darton, *J. Colloid Interface Sci.* **1999**, *215*, 323.
- [28] J. R. Clarkson, Z. F. Cui, R. C. Darton, *J. Colloid Interface Sci.* **1999**, *215*, 333.
- [29] T. Krause, B. Keshavarzi, J. Dressel, S. Heitkam, M. B. Ansorge-Schumacher, *Biotechnol. J.* **2022**, *17*, 2200271.
- [30] Z. Liu, Z. Liu, D. Wang, F. Ding, N. Yuan, *Bioseparation* **1998**, *7*, 167.
- [31] N. Brun, A. Babeau Garcia, H. Deleuze, M. F. Achard, C. Sanchez, F. Durand, V. Oestreicher, R. Backov, *Chem. Mater.* **2010**, *22*, 4555.
- [32] S. C. Reddington, M. Howarth, *Curr. Opin. Chem. Biol.* **2015**, *29*, 94.
- [33] S. L. Anna, *Annu. Rev. Fluid Mech.* **2016**, *48*, 285.
- [34] T. Fu, Y. Ma, *Chem. Eng. Sci.* **2015**, *135*, 343.
- [35] M. Grsche, A. E. Zoheir, J. Stegmaier, R. Mikut, D. Mager, J. G. Korvink, K. S. Rabe, C. M. Niemeyer, *Small* **2019**, *15*, 1901956.
- [36] M. Skoupi, C. Vaxelaire, C. Strohmman, M. Christmann, C. M. Niemeyer, *Chem.-Eur. J.* **2015**, *21*, 8701.
- [37] Y. Dai, C. Li, L. Zheng, B. Jiang, T. Zhang, J. Chen, *Biochem. Eng. J.* **2022**, *178*, 108303.
- [38] H.-J. Kim, S.-A. Ryu, P. Kim, D.-K. Oh, *Biotechnol. Prog.* **2003**, *19*, 400.
- [39] D.-W. Lee, H.-J. Jang, E.-A. Choe, B.-C. Kim, S.-J. Lee, S.-B. Kim, Y.-H. Hong, Y.-R. Pyun, *Appl. Environ. Microbiol.* **2004**, *70*, 1397.
- [40] H.-J. Oh, H.-J. Kim, D.-K. Oh, *Biotechnol. Lett.* **2006**, *28*, 145.
- [41] S. K. Rai, H. Kaur, B. S. Kauldhar, S. K. Yadav, *ACS Biomater. Sci. Eng.* **2020**, *6*, 6661.
- [42] S. K. Rai, H. Kaur, A. Singh, M. Kamboj, G. Jain, S. K. Yadav, *Biocatal. Agric. Biotechnol.* **2021**, *38*, 102227.
- [43] K.-C. Shin, M.-J. Seo, S. J. Kim, Y.-S. Kim, C.-S. Park, *Appl. Sci.* **2022**, *12*, 4696.
- [44] G. Zhang, H. M. Zabed, J. Yun, J. Yuan, Y. Zhang, Y. Wang, X. Qi, *Bioresour. Technol.* **2020**, *305*, 123010.
- [45] J.-J. Liu, G.-C. Zhang, S. Kwak, E. J. Oh, E. J. Yun, K. Chomvong, J. H. D. Cate, Y.-S. Jin, *Nat. Commun.* **2019**, *10*, 1356.
- [46] W. Liu, Z. Zhang, Y. Li, L. Zhu, L. Jiang, *Food Res. Int.* **2023**, *166*, 112637.
- [47] H. F. Son, S.-M. Lee, K.-J. Kim, *Sci. Adv.* **2018**, *8*, 17442.
- [48] Y. Carius, H. Christian, A. Faust, U. Zander, B. U. Klink, P. Kornberger, G.-W. Kohring, F. Giffhorn, A. J. Scheidig, *J. Biol. Chem.* **2010**, *285*, 20006.
- [49] S. S. Jagtap, R. Singh, Y. C. Kang, H. Zhao, J.-K. Lee, *Enzyme Microb. Technol.* **2014**, *58-59*, 44.
- [50] K. M. Polizzi, A. S. Bommarius, J. M. Broering, J. F. Chaparro-Riggers, *Curr. Opin. Chem. Biol.* **2007**, *11*, 220.
- [51] R. Greifenstein, T. Ballweg, T. Hashem, E. Gottwald, D. Achauer, F. Kirschhöfer, M. Nusser, G. Brenner-Weiß, E. Sedghamiz, W. Wenzel, E. Mittmann, K. S. Rabe, C. M. Niemeyer, M. Franzreb, C. Wöll, *Angew. Chem. Int. Ed. Engl.* **2022**, *61*, e202117144.